BIOCHEMISTRY
including biophysical chemistry & molecular biology
Article

Biochemistry **2010,** *49,* 9809–9819 9809
DOI: 10.1021/bi1011173

Alternative Sigma Factors in the Free State Are Equilibrium Mixtures of Open and Compact Conformations†

Paromita Raha,‡ Suranjana Chattopadhyay,§ Srijata Mukherjee,‡ Ruchira Chattopadhyay,‡ Koushik Roy,‡ and Siddhartha Roy*,‡

‡*Department of Structural Biology and Bioinformatics, Indian Institute of Chemical Biology, 4, Raja S.C. Mullick Road, Kolkata 700 032, India, and* §*Department of Biophysics, Bose Institute, P-1/12, CIT Scheme VII M, Kolkata 700 054, India*

Received July 13, 2010; Revised Manuscript Received October 3, 2010

ABSTRACT: Conformational switching upon core RNA polymerase binding is an integral part of functioning of bacterial sigma factors. Here, we have studied dynamical features of two alternative sigma factors. A study of fluorescence resonance energy transfer and hydrodynamic measurements in *Escherichia coli* σ^{32} suggest a compact shape like those found in complex with anti-sigma factors. On the other hand, the fluorescence anisotropy of probes attached to different regions of the protein and previous hydrogen exchange measurements suggest significant internal flexibility, particularly in the C-terminal half and region 1. In a homologous sigma factor, σ^{F} of *Mycobacterium tuberculosis*, emission spectra and fluorescence resonance energy transfer between the single tryptophan (W112) and probes placed in different regions suggest a compact conformation for a major part of the N-terminal half encompassing region 2 and the flexible C-terminal half. Fluorescence anisotropy measurements suggest significant flexibility in the C-terminal half and region 1, as well. Thus, free alternative sigma factors may be in equilibrium between two conformations: a compact one in which the promoter interacting motifs are trapped in the wrong conformation and another less abundant one with a more open and flexible conformation. Such flexibility may be important for promoter recognition and interaction with many partner proteins.

Bacterial sigma factors associate with the core RNA polymerase and turn on a set of genes. On the basis of representative experiments, it is generally believed that the free sigma factors are incapable of binding to promoters and acquire the ability to bind promoters with high specificity only as a part of the holoenzyme (*1*). The conformational nature of the sigma factors in these two states remains largely unknown, although this may be crucial to their function. Because the sigma factor as a part of the holoenzyme recognizes many different, but homologous, DNA sequences, it is likely that flexibility plays an important role in adaptation. The role of dynamics in the functioning of sigma factors, however, is not well understood. The alternative sigma factors may have a more stringent recognition property than the more promiscuous housekeeping sigma factors. The higher specificity of alternate sigma factors may necessitate more extensive promoter contacts and hence the ability to adapt to different sequences more effectively. Thus, dynamical features of these molecules may shed light on the mechanism of promoter recognition.

In primary sigma factors of the σ^{70} family, region 1.1 plays a crucial role in inhibition of the free sigma factor binding to promoters (*1*). Initially, it was thought that this region binds to region 4.2 (which interacts with the −35 region of the promoter) and prevents promoter binding (*2*). Recent NMR data and other results have now cast serious doubt on this hypothesis (*3*). Muir and co-workers have recently proposed that region 1.1 interacts intramolecularly with a compact conformation of the sigma factor in the free state in which regions 2.1 and 4.2 are not in the proper spatial relation for promoter binding (*4*, *5*). Such compact models of the native state of sigma factors may not possibly be the sole representation of the free state. In Ecσ^{32}, for example, amide protons of a large part of the C-terminal half show little protection from hydrogen−deuterium exchange in the native state (*6*). This suggests substantial flexibility and solvent exposure, at least transiently, of a large part of the protein. It is also well-known that sigma factors rarely form good crystals, and to the best of our knowledge, no whole sigma factor crystal structure is known, again suggesting considerable conformational flexibility. In addition, many sigma factors lack region 1.1 altogether, and how these sigma factors are prevented from binding to the promoters remains a mystery. Clearly, a deeper understanding of the conformational properties of sigma factors in the free state is desirable.

As amply demonstrated in the past, many regulatory proteins are not rigid (*7*). In fact, a large number of them are probably highly flexible and perhaps partially disordered. The role of disorder in specific interactions is just beginning to be understood. We felt that a study of the dynamical properties of free sigma factors may play a crucial role in the understanding of the conformational switch. In this work, we report the study of dynamical properties of two alternative sigma factors, σ^{32} of *Escherichia coli* and σ^{F} of *Mycobacterium tuberculosis*, in the free state and its implications for promoter recognition. The two sigma factors studied here have similar functions in the two organisms. *E. coli* σ^{32} is involved in the heat-shock response, whereas *M. tuberculosis* σ^{F} is also probably involved in heat-shock and other stress responses.

†This work was supported by the Council of Scientific and Industrial Research (India) and a J. C. Bose Fellowship to S.R.

*To whom correspondence should be addressed. Telephone: 91-33-2413-1157. Fax: 91-33-2473-5197. E-mail: sidroykolkata@gmail.com.

Published on Web 10/05/2010

EXPERIMENTAL PROCEDURES

Materials. Ampicillin, carbenicillin, kanamycin, IPTG,[1] PMSF, DTT, EDTA, and DTNB were purchased from Sigma Chemical Co. Bacto-tryptone, bacto-agar, and yeast extract were purchased from Hi-Media. Anhydrous glycerol was purchased from J. T. Baker; 4× crystallized acrylamide and Tris-HCl were purchased from Spectrochem. IAF and IAEDANS were purchased from Molecular Probes Inc. Ni-NTA agarose was purchased from Qiagen. The primers for the PCR amplification reaction were obtained from Isogen Inc. Restriction endonucleases were purchased from New England Biolabs Inc. Plasmids pGEM3Z, pGEX6P1, pQE30, pET28a, and pREP4 were obtained from Promega, Amersham-Pharmacia Biotech, Novagen, and Qiagen. All other reagents were of analytical grade.

Cloning and Purification of Mtσ^F. The Mtσ^F gene was amplified by polymerase chain reaction using appropriately designed complementary primers from the H37Rv strain DNA of *M. tuberculosis* and cloned in the *Bam*HI site of the pUC18 cloning vector. This was then subcloned into the *Bam*HI site of the pET28a expression vector. The gene was fully sequenced. The plasmid encoding the protein was transformed in BL21(DE3) competent cells. The transformed cells were grown in Luria broth containing 50 μg/mL kanamycin at 37 °C until the absorbance at 600 nm reached 0.3. The culture was then cooled to 16 °C, induced with 0.25 mM IPTG, and grown for 16−18 h at this temperature. The harvested cells were then resuspended in lysis buffer comprising 50 mM potassium phosphate buffer (pH 8.0) containing 300 mM KCl, 10 mM imidazole, 5% glycerol, 1 mM β-mercaptoethanol, 1 mM PMSF, and 0.1% Triton X-100 and lysed by sonication. The cell debris was then removed by centrifugation at 12000 rpm for 40 min. The supernatant was then loaded onto a Ni-NTA agarose column pre-equilibrated with lysis buffer. Binding was allowed for 1 h, after which two subsequent washings were conducted with 50 mM potassium phosphate buffer (pH 8.0) containing 300 mM KCl and 20 mM imidazole, followed by 50 mM imidazole in the same buffer. The protein was eluted with an imidazole gradient from 50 to 350 mM in 50 potassium phosphate buffer (pH 8.0) containing 300 mM KCl, 20% glycerol, and 1 mM β-mercaptoethanol. The fractions were then pooled together and dialyzed against storage buffer, which consisted of 50 mM Tris-HCl buffer (pH 8.0) containing 200 mM KCl, 20% glycerol, 10 mM $MgCl_2$, and 1 mM β-mercaptoethanol, and stored in aliquots at −80 °C.

Site-Directed Mutagenesis, Cloning, and Purification of the Mtσ^F Mutants. The N-terminal mutant genes of A6C/C47A-Mtσ^F and V19C/C47A-Mtσ^F and the C-terminal mutant genes of L256C/C47A-Mtσ^F were made via the PCR-based overlap extension procedure (*8*) using two mutagenic primers and outside primers with *Bam*HI and *Sal*I restriction sites and high-fidelity Pfu polymerase. All the mutants were first cloned in the pUC18 cloning vector, sequenced, and then subcloned in the pQE30 expression vector. The plasmids encoding the mutant proteins were transformed into XL1 Blue competent cells. The transformed cells were grown in Luria broth containing 100 μg/mL ampicillin at 37 °C until the absorbance at 600 nm reached 0.3. The culture was then cooled to 16 °C, induced with 0.25 mM IPTG, and grown for 16−18 h at this temperature. The mutant proteins were purified using the same protocol that was used for wild-type Mtσ^F. In some preparations of the mutant Mtσ^F, a minor band with a slightly higher molecular weight was sometimes observed. Mass spectrometric analysis suggests that this band may originate from a read-through of the stop codon (*9*).

Site-Directed Mutagenesis of Ecσ^{32}. The N-terminal mutant gene M5C-Ecσ^{32} was constructed using two mutagenic primers and outside primers containing *Eco*RI and *Sal*I restriction sites and high-fidelity Pfu polymerase. After PCR, the product was digested with *Eco*RI and *Sal*I and cloned in the pGEX-6P1 vector to give us the recombinant plasmid DNA carrying the M5C-Ecσ^{32} gene. Similar procedures were used for all other single-cysteine mutants except the final expression plasmid was pQE30. For construction of the double mutant LV37,262CC-Ecσ^{32} gene, the L37C-Ecσ^{32} gene in the pGEM3Z plasmid was amplified further by the overlap extension method using appropriate mutagenic primers for introduction of the V262C mutation. After restriction digestion and cloning in pGEM3Z, the gene was further subcloned into pQE30. All the mutant genes were fully sequenced.

Purification of M5C-Ecσ^{32}. A 3 L culture was grown after the cloned vector M5C-Ecσ^{32}-pGEX6P1 had been freshly transformed in CG410 (DnaK Δ756 mutant *E. coli* strain), in 2×YT medium with carbenicillin at 30 °C. The cells were grown until A_{600} reached 0.5, and 0.5 mM IPTG was added and the mixture shaken for a further 1 h and harvested. Cells were sonicated by being suspended in 60 mL of PBSX buffer [1× PBS (pH 7.4) containing 50 mM L-phenylalanine, 50 mM L-isoleucine, 1 mM β-mercaptoethanol, and 1 mM PMSF]. The sonicated mass was centrifuged at 12000 rpm for 45 min at 4 °C. After the supernatant had been diluted to 100 mL with PBSX buffer, it was loaded onto a 4 mL Glutathione Sepharose 4B (Amersham Pharmacia Biotech) column pre-equilibrated with 40 mL of PBSX buffer. Then the column was washed with 40 mL of PBSX buffer, followed by 15 mL of cleavage buffer X [50 mM Tris-HCl buffer (pH 7.0) containing 150 mM NaCl, 1 mM EDTA, 1 mM DTT, 50 mM phenylalanine, and 50 mM isoleucine]; 40 μL of PreScission Protease (Amersham Pharmacia Biotech) per bed volume was added to the column material (containing the bound protein) resuspended in 12 mL of cleavage buffer X. It was incubated for 10 h at 4 °C. The column material was then repacked, and the eluate was collected in 1.5 mL fractions. It was further eluted with 10 mL of cleavage buffer X in 1.5 mL fractions. The purified M5C-Ecσ^{32} protein was thus separated from GST via dialysis in 1 L of storage buffer [50 mM potassium phosphate buffer (pH 7.9) containing 300 mM KCl, 25% glycerol, and 1 mM β-mercaptoethanol] and stored at −20 °C.

Purification of Other Ecσ^{32} Mutants. The purification was conducted according to the method of Joo et al. (*10*) with several modifications. The CG410 strain containing pQE30 carrying the H107C-Ecσ^{32} gene and pREP4 plasmids was grown at 30 °C in 1 L of 2×YT medium with 100 μg/mL ampicillin and 50 μg/mL kanamycin. At an appropriate A_{600}, IPTG was added to a final concentration of 0.5 mM. The cells were grown for an additional 20 min and poured into tubes of ice. All of the subsequent steps were performed at 4 °C. After centrifugation at 5000 rpm for 10 min, the cell pellet was resuspended in 18 mL of ice-cold buffer X [50 mM phosphate buffer (pH 7.9) containing 300 mM KCl, 50 mM isoleucine, 50 mM phenylalanine, and 1 mM

[1]Abbreviations: Ecσ^{32}, sigma 32 from *E. coli*; Mtσ^F, sigma F from *M. tuberculosis*; FRET, fluorescence resonance energy transfer; IAEDANS, 5-({2-[(iodoacetyl)amino]ethyl}amino)naphthalene-1-sulfonic acid; IAF, 5-iodoacetamido fluorescein; Ttσ^{70}, sigma 70 of *Thermus thermophilus*; IPTG, β-isopropyl thiogalactoside; Aaσ^{28}, sigma 28 from *Aquifex aeolicus*; PMSF, phenylmethanesulfonyl fluoride; DTT, 1,4-dithiothreitol; EDTA, ethylenediaminetetraacetic acid; DTNB, 5,5′-dithiobis(2-nitrobenzoic acid); TCEP, tris(2-carboxyethyl)phosphine hydrochloride.

β-mercaptoethanol] containing 20 mg/mL PMSF and disrupted by sonication. The cell lysate was centrifuged for 45 min at 12000*g*. The supernatant was loaded onto a 3 mL Ni-NTA-agarose column pre-equilibrated with buffer X at a rate of 0.4 mL/min. The column was subsequently washed with 40 mL of buffer X and then with 10 mL of buffer X containing 15 mM imidazole. Nickel-bound proteins were eluted with 30 mL of a 15 to 150 mM imidazole gradient in buffer X. Pure fractions of Ecσ^{32} proteins were dialyzed against two changes of 1 L of 50 mM phosphate buffer (pH 7.9) containing 300 mM KCl and 50% glycerol. All other site-directed Ecσ^{32} mutants were purified by a similar purification protocol.

Chemical Modification of Single-Cysteine Mtσ^F Mutants. The A6C-Mtσ^F mutant was labeled with IAF. Prior to being labeled, the protein was dialyzed against 1 L of degassed 50 mM potassium phosphate buffer (pH 7.5) containing 300 mM KCl, 1 mM EDTA and 20% glycerol. Labeling of the protein with IAF was achieved via incubation of the protein at 7.5 μM with a 20-fold molar excess of IAF at 25 °C for 4 h with continuous stirring in the same buffer. The protein was then extensively dialyzed in same buffer containing 1 mM β-mercaptoethanol for removal of excess probe. Similar protocols were used for L256C/C47A-Mtσ^F and V19C/C47A-Mtσ^F for IAF as well as IAEDANS labeling.

Chemical Modification of Ecσ^{32} Mutants. The H107C-Ecσ^{32} mutant was labeled with IAF. Prior to labeling, the protein was dialyzed against 1 L of degassed 50 mM potassium phosphate buffer (pH 7.5) containing 300 mM KCl, 1 mM EDTA, and 20% glycerol. Labeling of the protein with 5-IAF was achieved via incubation of the protein at 10 μM with a 20-fold molar excess of IAF at 25 °C for 4 h with continuous stirring in 50 mM potassium phosphate buffer (pH 7.5) containing 300 mM KCl, 1 mM EDTA, and 20% glycerol. The protein was then extensively dialyzed in the same buffer containing 1 mM β-mercaptoethanol for removal of excess probe. The incorporation ratio was determined using an ε_{490} of 80000 M^{-1} cm^{-1} (*11*). The protein concentration was determined from absorbance values at 280 nm after subtraction of the contribution from IAF.

For anisotropy measurements, the purified M5C-Ecσ^{32} was first dialyzed at 4 °C in degassed buffer [50 mM potassium phosphate buffer (pH 7.9) containing 300 mM KCl, 20% glycerol, and 1 mM EDTA]. It was then labeled via addition of a 5-fold molar excess of IAEDANS to 0.9 mg/mL protein and incubation at 37 °C in a water bath for 2 h. The reaction was quenched with 1 mM β-mercaptoethanol and the mixture further dialyzed in 4 L of the same buffer (containing 15% glycerol, 0.5 mM EDTA, and 1 mM β-mercaptoethanol), sequentially with five changes over day and night to remove the excess fluorophore. All other mutants were labeled similarly. For double labeling of the double mutant, the LV37,262CC-Ecσ^{32} mutant protein was dialyzed in degassed buffer [50 mM potassium phosphate buffer (pH 7.9) containing 300 mM KCl, 25% glycerol, and 1 mM EDTA] followed by addition of a 0.8-fold molar ratio of IAEDANS to 0.7 mg/mL protein and incubation at 37 °C in a water bath for 2 h. The reaction was quenched with 1 mM β-mercaptoethanol and the mixture further dialyzed against 4 L of the same buffer (containing 0.5 mM EDTA and 1 mM β-mercaptoethanol), sequentially with five changes over day and night to remove excess fluorophore (IAEDANS). The resulting labeled protein exhibited 80% incorporation of IAEDANS. In the next stage, the IAEDANS-labeled mutant protein was used, and a 10-fold molar excess of IAF was added to it and the mixture stirred at room temperature for 1 h. The reaction was quenched using 1 mM β-mercaptoethanol and the mixture dialyzed extensively in the same buffer with several changes for 48−72 h until all the excess fluorophore was removed. The level of incorporation was 50% for IAF.

Circular Dichroism. The measurements were taken with a JASCO-J720 spectropolarimeter at 30 °C, in a cuvette with a path length of 0.3 cm. The protein was kept at 3 μM in 0.05 M potassium phosphate buffer (pH 8.0) containing 0.2 M KCl and 20% glycerol.

Steady-State Fluorescence Measurements. All fluorescence spectra were recorded in Quantamaster 6 (PTI) T-geometry spectrofluorometer or Perkin-Elmer LS55 spectrofluorometer. The excitation and emission band-passes were set at 5 nm for all measurements, unless stated otherwise. The tryptophan emission scans of wild-type Mtσ^F and its mutants, A6C/C47A-Mtσ^F, V19C/C47A-Mtσ^F, and L256C/C47A-Mtσ^F, were taken at protein concentrations of 4.2, 5, 3, and 4 μM, respectively. The proteins were taken in 0.05 M Tris-HCl buffer (pH 8.0) containing 0.2 M KCl and 20% glycerol. The excitation wavelength was set at 295 nm, and each spectrum was the average of three scans.

Acrylamide Quenching of Mtσ^F and L256C/C47A-Mtσ^F. For acrylamide quenching of tryptophan fluorescence, to a protein concentration of 5 μM in 0.05 M potassium phosphate buffer (pH 8.0) containing 0.2 M KCl, 20% glycerol, 0.5 mM EDTA, and 1 mM β-mercaptoethanol, acrylamide from a freshly prepared 1 M stock in the same buffer was added to the protein solution at intervals of 5 mM to a final concentration of 100 mM. At each acrylamide concentration, the fluorescence intensity was measured. The excitation wavelength was set at 295 nm, and the emission wavelengths were set at 341 and 343 nm for wild-type Mtσ^F and mutant L256C/C47A-Mtσ^F, respectively. The experiments were performed at 25 °C, and the temperature was maintained with a circulating water bath attached to the spectrofluorometer. The observed fluorescence values were corrected for the inner filter effect using the formula

$$F_{corr} = F_{obs}\ \text{antilog}[(A_{ex} + A_{em})/2]$$

where the *A* terms are the absorbances at the excitation and emission wavelengths and the *F* values are the corrected and observed fluorescence intensities. Absorbance at the excitation and emission wavelengths was measured before and after titration, and intermediate values were obtained by interpolation. Appropriate blank spectra were always subtracted from the actual spectra. The data were fitted to the Stern−Volmer equation. Collisional quenching of fluorescence is described by the Stern−Volmer equation

$$F_0/F = 1 + K_{sv}[Q]$$

where F_0 and F are the fluorescence intensities in the absence and presence of quencher, respectively, and K_{sv} represents the Stern−Volmer constant.

Perrin Plot. To determine the correlation time and limiting anisotropy, an isothermal Perrin plot was created. The Perrin equation is given as

$$1/A = 1/A_0(1 + \tau_f/\tau_c) = 1/A_0(1 + \tau_f kT/V_h\eta)$$

where τ_f is the fluorescence lifetime, τ_c is the rotational correlation time, k is the Boltzmann constant, T is the temperature, V_h is the molecular volume, and η is the viscosity of the solution. The viscosity was varied isothermally (25 °C) with increasing

concentrations of glycerol in 0.05 M potassium phosphate buffer (pH 8.0). Literature values for the viscosity of glycerol from the *Handbook of Chemistry and Physics* (*12*) were used. The excitation wavelength was 490 nm, and the emission wavelength was 525 nm. The IAF-labeled A6C/C47A-Mtσ^F concentration was kept at 0.14 μM. The IAF-labeled H107C-Ecσ^{32} concentration was kept at 0.25 μM. Similar protocols were followed for other mutants.

Sedimentation Equilibrium. To determine the molar mass of Mtσ^F and Ecσ^{32}, sedimentation equilibrium measurements were taken in a Beckman Coulter XL-I analytical ultracentrifuge. The experiment was performed at a temperature of 20 °C. The speed was set at 9000 rpm, and an equilibrium run was continued for 72 h. The protein concentration was kept at 2 μM in 0.02 M Tris-HCl buffer (pH 8.0) containing 0.2 M KCl, 0.01 M $MgCl_2$, and 20% glycerol. The exponential distribution at sedimentation equilibrium is the sum of the exponentials of the macromolecular species present in solution where the concentration of each component varies exponentially with $r^2/2$ as a function of $M_n(1 - v_n\rho)\omega^2/2RT$ according to the equation

$$M_n(1 - v_n\rho) = [\mathrm{d}\ \ln(c)/\mathrm{d}r^2](2RT/\omega^2)$$

where r denotes the radius, M_n is the molar mass, v_n is the partial specific volume, ρ is the density, ω is the angular velocity, and T is the temperature. A plot of ln C versus $r^2/2$ allows one to determine M directly.

Measurements of Mtσ^F Lifetimes. For Mtσ^F and its mutants, the tryptophan lifetime was measured in a Quantamaster 6 (PTI) T-geometry spectrofluorometer with an Easy-Life Lifetime System using a solid-state pulsed laser. The labeled and unlabeled protein concentrations were kept at 3.5 μM for each of the proteins mentioned above in 0.05 M potassium phosphate buffer (pH 8.0) containing 0.2 M KCl, 0.5 mM EDTA, 10% glycerol, and 1 mM β-mercaptoethanol. The time-resolved readings were taken by setting the excitation and emission wavelengths to 280 and 340 nm, respectively. The scans were collected over 200 channels with start and end times of 55 and 155 ns, respectively. An average of 20 such scans was taken for each measurement. The tryptophan lifetimes of the unlabeled (donor) and labeled proteins (donor−acceptor) were thus used to calculate the efficiency of the transfer of energy between W112 and Cys-AEDANS at the different positions of the protein according to the following equation:

$$E = 1 - \tau_{DA}/\tau_D$$

Time-Resolved Anisotropy Decay Experiments. For the time-resolved anisotropy decay experiment with Ecσ^{32}, the labeled protein sample (5 μM) was excited at 336 nm using a picosecond diode laser (IBH nanoled-07) with a pulse width of 70 ps at a repetition rate of 800 kHz. The fluorescence was dispersed using a monochromator (Applied Photophysics; $f = 3.4$). The exciting laser beam scattered by the sol−gel sample was blocked using a Melles Griot filter. The fluorescence decays were collected at magic angle polarization using an analyzer and a Hamamatsu MCP photomultiplier (2809U). The time-correlated single-photon counting (TCSPC) setup consisted of an ortec 935 QUAD CFD and a tennelec TC 863 TAC. The data were collected with a PCA 3 card (oxford) as a multichannel analyzer. The fluorescence decays were deconvoluted using global lifetime analysis software (Photon Technology International) in which both the lifetimes and amplitudes of the individual decays were allowed to vary freely. For Mtσ^F, the mutant proteins were labeled with Alexa Fluor 488 C_5-maleimide. Prior to being labeled, the protein was incubated with 1 mM TCEP for 1 h at 4 °C in 50 mM potassium phosphate buffer (pH 7.5) containing 300 mM KCl, 1 mM EDTA, and 20% glycerol. Labeling of the protein with Alexa Fluor 488 C_5-maleimide was achieved via incubation of the protein at 10 μM with a 10-fold molar excess of Alexa Fluor 488 C_5-maleimide at 25 °C for 4 h with continuous stirring in the same buffer. The protein was then extensively dialyzed in the same buffer containing 1 mM β-mercaptoethanol for removal of excess probe. The protein concentration was 0.3 μM.

Steady-State Fluorescence Resonance Energy Transfer Experiment. IAEDANS was used as the donor and IAF as the acceptor in the FRET experiment; 500 μL of 1 μM doubly labeled mutant protein was taken in the 50 mM potassium phosphate buffer (pH 7.9) containing 300 mM KCl and 25% glycerol, and its fluorescence intensity was scanned through the 310−550 nm range. The emission wavelength was fixed at 570 nm. The bandpasses of the slits were kept at 5 nm each. Direct donor excitation was subtracted from the spectra by taking the excitation spectra of the cysteine conjugate of IAEDANS.

The efficiency of energy transfer was calculated from the following equation:

$$\frac{F_{D+A}}{F_A} = 1 + \frac{\varepsilon_D C_D}{\varepsilon_A C_A} E$$

where E is the efficiency of FRET, F_{D+A} is the fluorescence intensity of the donor- and acceptor-labeled mutant protein at 335 nm that is actually $F_{(D+A)obs} - F_{Dobs}$, F_A is the fluorescence intensity of the acceptor at 335 nm, ε_D is the molar extinction coefficient of the donor (IAEDANS) (which is 5700 M^{-1} cm^{-1}), ε_A is the molar extinction coefficient of the acceptor (IAF) at the absorption maxima (336 nm) of the donor (which is 9000 M^{-1} cm^{-1}), and C_D and C_A are the concentrations of the donor and acceptor, respectively. Energy transfer efficiency E is related to distance by the following equation:

$$E = [1 + (R/R_0)^6]^{-1}$$

where R_0 is the distance at 50% E. The energy transfer efficiency was corrected for partial labeling. R_0 was calculated according to the method of Bhattacharyya et al. (*13*).

Homology Modeling. The crystal structure of σ^{70} of *Thermus thermophilus* (Protein Data Bank entry 1IW7, chain F) was used as a template. It was 29% identical to Ecσ^{32}. It was found that residues 74−423 of the amino acid chain of 1IW7F (sigma 70 of *T. thermophilus*) matched correctly with the sequence of Ecσ^{32}. Mtσ^F modeling was performed by automatic homology modeling on the Swiss Model Web server on an Aaσ^{28} template (Protein Data Bank entry 1RP3).

RESULTS

It is well-known that free sigma factors do not bind to promoters. This is perhaps vital for the cell so that the free sigma factors do not compete for the promoters with the holoenzyme. For primary sigma factors of the σ^{70} family, it is believed that N-terminal region 1.1 plays a crucial role in inhibiting the free proteins from binding to the promoters. The exact mechanism of this inhibition is still not clear. A proper understanding of the mechanism of the lack of promoter binding by sigma factors in

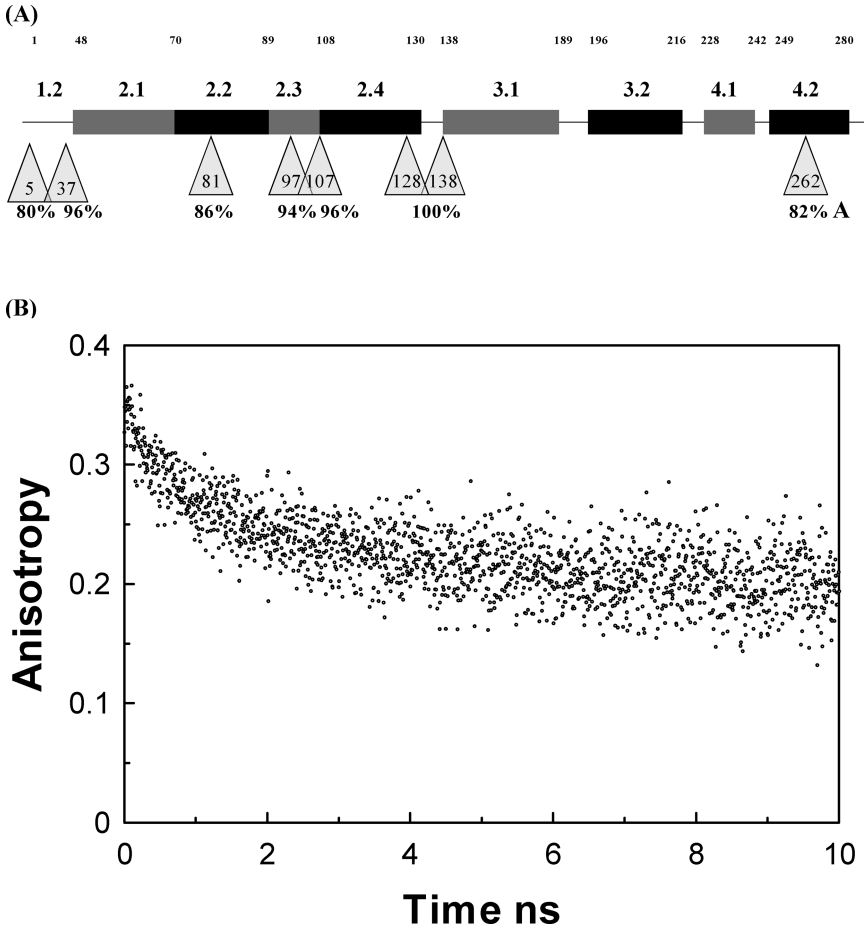

FIGURE 1: (A) Steady-state fluorescence anisotropy values of IAEDANS placed at different regions of Ecσ^{32} given as a percentage of the highest observed anisotropy (bottom most row of numbers), that of residues 128 and 138. The measurement temperature was 37 °C. Protein concentrations were 1 μM. Excitation and emission wavelengths were 336 and 482 nm, respectively. Band-passes were 5 nm each. The measurements were taken in 0.05 M potassium phosphate (pH 7.9) containing 300 mM KCl and 25% glycerol. The top numbers are domain boundaries. Larger fonts in the second row represent domain identity as derived from ref *15*. The numbers within the lower triangles represent site-directed single-cysteine mutants. (B) Time-resolved anisotropy decay of M5C-AEDANS-Ecσ^{32}. The protein concentration was 5 μM in binding buffer [20 mM Hepes buffer (pH 7.6) containing 100 mM NaCl, 5 mM DTT, 0.1 mM EDTA, and 25% glycerol].

the free state may be appreciated if one investigates the conformational properties of sigma factors. Structural interpretations are, however, far easier if a high-resolution structure of the protein or its close homologue is known. Aaσ^{28} and its homologous sigma factors perhaps offer the best possibility in this respect as the crystal structure of the Aaσ^{28}−FlgM complex has been elucidated (*14*).

Phylogenetic relationships described by Paget and Helmann (*15*) place Aaσ^{28} in group 3. This group contains several other closely related subgroups. We have chosen Ecσ^{32} and Mtσ^{F} from different subgroups of group 3 for further study and compared the structure and dynamics of these sigma factors with those of Aaσ^{28}. One of the reasons for choosing Ecσ^{32} is based on the demonstrated fact that the first 49 residues of Ecσ^{32} inhibit free Ecσ^{32} from binding to promoters (*1*). Deletion of this region (residues 1−49) removes the inhibition. This region, however, does not align with region 1.1 of primary sigma factors (*16*), but with region 1.2. Mtσ^{F} has an N-terminal extension (residues 1−39), comparable to residues 1−49 of Ecσ^{32}, but having little sequence similarity (data not shown). To understand the structural basis of inhibition of promoter binding by residues 1−49 (region 1.2), we first studied the conformational dynamics of Ecσ^{32}.

Dynamic Nature of Sigma Factor Ecσ^{32}. In a previous article, Rist et al. (*6*) examined the hydrogen−deuterium exchange rates of amide protons throughout the length of Ecσ^{32} as a function of temperature. Interestingly, many of the amide protons from the C-terminal half show far less protection from solvent exchange when compared to most of the N-terminal half, suggesting enhanced exposure. To better understand the dynamical nature of free Ecσ^{32}, we have created a series of site-directed cysteine mutants, spanning the whole length of the protein. Wild-type Ecσ^{32} has no cysteine residue, and hence, all the mutant proteins are single-cysteine proteins (except where mentioned otherwise). One of the mutant proteins studied, BB4708, contained two cysteine residues at positions 128 and 138 (*17*). However, only one cysteine is reactive and becomes labeled, but the identity of the cysteine residue is not known. An engineered mutant reported here, L37C/V262C-Ecσ^{32}, also has two cysteines. However, the two cysteines in this double mutant react with greatly different rates (Figure 1 of the Supporting Information), with 262C reacting almost instantaneously (estimated $t_{1/2}$ of ~2 min) and 37C reacting with a $t_{1/2}$ of 38 min. The reaction rates were assigned from the slowness of the reaction of L37C-Ecσ^{32} (data not shown). This allows selective labeling of 262C in the double mutant. If all the mutant Ecσ^{32} forms were labeled with the same probe (IAEDANS), and its anisotropy examined, the differences in anisotropy value would qualitatively reflect the relative flexibility of different regions of the protein as the overall tumbling motions remain the same. Figure 1A shows the domain structure

of Ecσ^{32}, the positions of different cysteine mutant proteins used in this study, and the anisotropy of Ecσ^{32} labeled at those positions. It is clear that the highest anisotropies are seen in and around region 2 and are significantly lower in either region 1 (residue 5) or near region 4.2 (residue 262). It is possible that site-directed mutagenesis and probe attachments may cause local changes in flexibility. However, the general trends obtained here are generally consistent with the results obtained from the H−D exchange experiment, suggesting no untoward effect of mutagenesis and probe attachment. It also suggests that region 2 contains a relatively rigidly folded domain and enhanced flexibility for region 4.2, as well as extremities of region 1.2.

To elucidate the true nature of flexibility in these regions, we have studied anisotropy decay of a probe attached to cysteine 5 in a site-directed mutant M5C-Ecσ^{32}. Figure 1B shows the anisotropy decay of AEDANS-labeled M5C-Ecσ^{32} in buffers containing 25% glycerol. Previously, we have shown that such high concentrations of glycerol are necessary to keep the protein active for a long period of time at room temperature, which is necessary for data collection for steady-state and time-resolved anisotropy experiments (*17*). Use of such a high concentration of glycerol probably slows some of the motions because of the solvent viscosity effect. The decay starts from the theoretical high value of 0.4 and declines to ~0.2 within 2 ns and then shows a slower decline. We interpret the data to mean that the second longer decay is due to overall tumbling of the protein (slowed by the high viscosity of 25% glycerol), and the first more rapid motion is that of the low-amplitude internal motion, including probe motion. This motion only averages out a part of the anisotropy, indicating the limited amplitude of this motion. Clearly, the extreme end of region 1.2 is not completely free to rotate and is possibly interacting with the folded domain in the N-terminal half.

Intramolecular FRET in Ecσ^{32}. Use of FRET in the study of distances in sigma factors was pioneered by Heyduk and co-workers (*18*). To understand the spatial relationship of the C-terminal half vis-à-vis the N-terminal domain, we have attempted to measure the distance between residue 37 (end of region 1.2) and residue 262 (region 4.2). These residues were labeled with a fluorescence donor (IAEDANS) and acceptor (IAF), and energy transfer was measured. Figure 2 shows the excitation spectra of the doubly labeled Ecσ^{32} in comparison with the same protein in 5 M GuHCl. Previously, we have shown that the protein is completely unfolded in 5 M GuHCl and, thus, should not show any significant FRET (*17*). As is apparent from the figure, there is significant energy transfer as the excitation spectrum in the native state has a significantly higher intensity around 340−350 nm (IAEDANS absorption band) when compared to the completely unfolded protein at 5 M GuHCl (*17*). The calculated energy transfer efficiency is 39%, corresponding to a distance of ~42 Å. Upper and lower limits calculated from steady-state anisotropies by the method of Lakowicz are 53.3 and 37.1 Å, respectively (*19*). Because the interpretation of the distances in terms of structure of the whole protein is dependent on the quaternary structure of the protein in solution, we have measured the molecular mass of Ecσ^{32} by the sedimentation equilibrium method. Figure 3A shows the ln C versus $r^2/2$ plot. The calculated molecular mass from the slope of the plot is 33.6 kDa, indicating the protein is monomeric under the solution conditions used.

To understand the implications of the measured distance by FRET for the structure and dynamics of the free protein, we have homology modeled Ecσ^{32} on Ttσ^{70} (Protein Data Bank entry 1IW7) template as in the holoenzyme structure (*20*) (Figure 4A,B). The basic characteristics of the modeled structure are similar to those of the other homology-modeled structure (*6*) of Ecσ^{32}. The α-helix content of this structure is 62% as determined by STRIDE (*21*). From the circular dichroism spectra obtained in a previous study (*17*), the estimated helix content is 52% (*22*, *23*). In this structure, the distance between residues 37 and 262 is

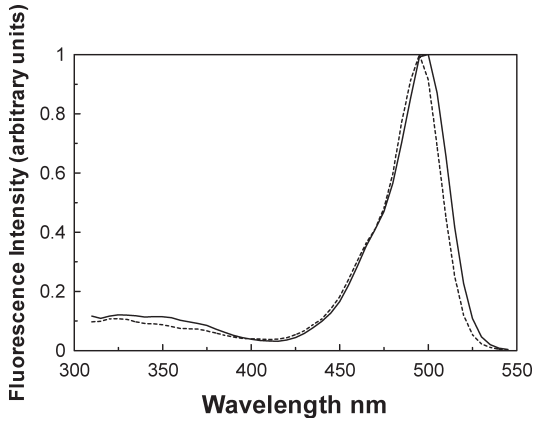

FIGURE 2: Fluorescence resonance energy transfer between residue 262C-AEDANS and 37C-AF in the double mutant LV37,262CC-Ecσ32. Comparison of excitation spectra of AF-37C and AEDANS-262C-Ecσ^{32} in the presence (···) and absence (—) of 5 M GuHCl. The protein concentration was 1 μM. The emission wavelength was 570 nm. The experiments were performed in 50 mM potassium phosphate buffer (pH 7.9) containing 300 mM KCl and 25% glycerol.

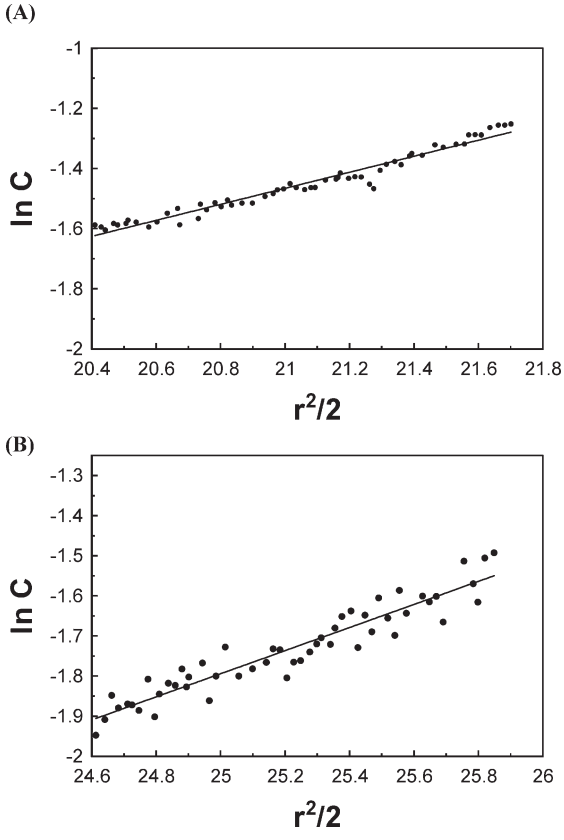

FIGURE 3: Plot of ln C vs $r^2/2$ for (A) Ecσ^{32} and (B) Mtσ^{F}. The sedimentation equilibrium run was conducted in a Beckman-Coulter XL-I analytical ultracentrifuge. The protein concentration was kept at 2 μM in 0.02 M Tris-HCl buffer (pH 8.0) containing 0.2 M KCl, 0.01 M $MgCl_2$, and 20% glycerol. The experiment was conducted at 20 °C at a speed of 9000 rpm, and the run was continued for 72 h. The absorbance was monitored at 230 nm.

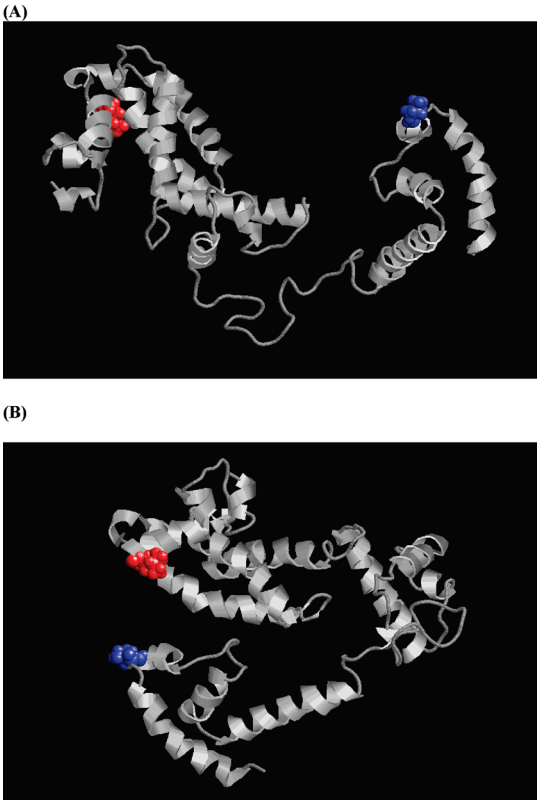

FIGURE 4: Homology-modeled structures of Ecσ32. (A) Structure based on the conformation of Ttσ^{70} in the holoenzyme. (B) Structure obtained after rotation around peptide bond 199. Residue 37 is colored red and residue 262 blue.

approximately 65 Å. Clearly, even the upper distance limit (53 Å) obtained from FRET is inconsistent with a totally open structure. We explored whether a closed Aaσ^{28}-like structure (*14*) can be produced from this with a minimum perturbation. Interestingly, just one rotation around peptide bond 199 produced a Aaσ^{28}-type closed structure in which the distance between residues 37 and 262 is reduced to 37 Å. This distance is compatible with the lower distance limit derived from FRET.

The two modeled conformations are likely to have very different hydrodynamic properties. We have thus attempted to construct a Perrin plot with Ecσ^{32} labeled at a residue in the well-folded part of the protein, very near region 2.4. This was done by labeling H107C-Ecσ^{32} with IAF and then constructing the Perrin plot (Figure 5). The plot is very linear with a *Y*-axis intercept of ~4. Although this value is somewhat higher than the theoretical limit of 2.5, the theoretical limit is rarely reached even for rigid proteins (*24*). Previous studies indicate that this value is consistent with a limited probe motion (*25*). The obtained rotational correlation time from the slope of the plot for H107C-Ecσ^{32} is 11.2 ns. This value is very close to the expected rotational correlation time of a spherical globular protein with a molecular mass of 32 kDa (*26*). Importantly, it appears that the protein tumbles as a whole, indicating a lack of major disorder. To verify that the protein is nearly spherical, we have determined the sedimentation coefficient of the protein in the absence of glycerol. The obtained $s_{20,w}$ is 4.2 S, very close to the expected value for a spherical molecule of this size (*26*). Hydrodynamic and FRET measurements thus clearly indicate that the protein is in a compact, nearly spherical conformation in which the C-terminal part is juxtaposed next to the N-terminal domain. However, the additional flexibility deduced from reduced anisotropy values of

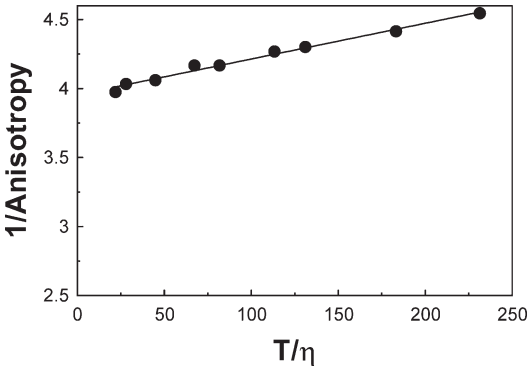

FIGURE 5: Perrin plot of AF-H107C-Ecσ^{32}. The protein concentration was kept at 0.25 μM for each reading. The viscosity was varied isothermally (25 °C) by inclusion of glycerol in 0.05 M potassium phosphate buffer (pH 8.0). The excitation wavelength was 490 nm, and the emission wavelength was 525 nm.

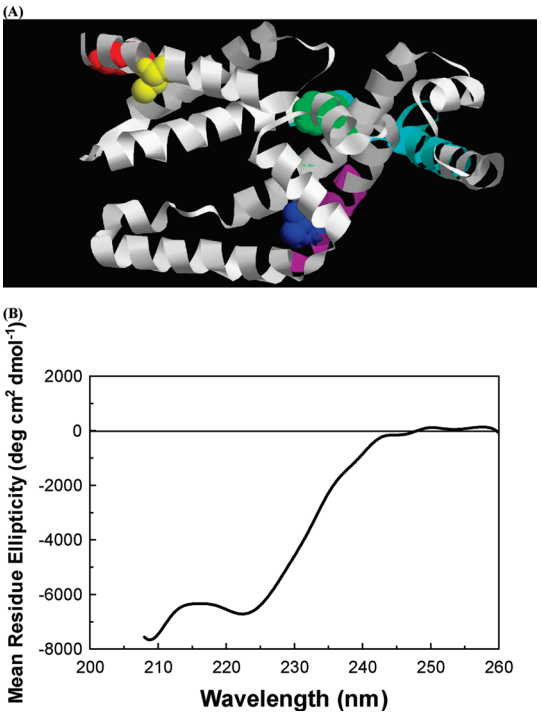

FIGURE 6: Homology-modeled structure of Mtσ^{F}. (A) The depicted structure shows the important residues. The residues are colored as follows: green for W112, blue for L256, yellow for C47, and red for R40. Region 2.4 (cyan) and region 4.2 (magenta) are marked. (B) Far-UV circular dichroism spectra of Mtσ^{F}. The path length of the cuvette was 0.3 cm. The solution conditions are given in Experimental Procedures.

the probes in certain regions of the protein and faster H−D exchange in the C-terminal half seen in a previous study (*6*) reflect either local or more global segmental flexibility of the C-terminal domain within the overall constraints of the compact tertiary structure of the protein.

Homology-Modeled Structure of Mtσ^{F}. Is this largely compact structure of Ecσ^{32} and Aaσ^{28} valid for other sigma factors? As stated before, we have chosen Mtσ^{F} for comparative study. Because Aaσ^{28} is evolutionarily closely related to Mtσ^{F}, we have homology modeled Mtσ^{F} on Aaσ^{28} structure (*14*). Figure 6 shows the homology-modeled structure of Mtσ^{F}. In this structure, the extreme N-terminal region is missing as the structure of the comparable region is absent in the crystal structure of Aaσ^{28}.

Table 1: Fluorescence Energy Transfer and Estimated Distances between W112 and Several Cysteines

protein	lifetime (ns)[a]	E	R (Å)[b]	R_{max} (Å)[c]	R_{min} (Å)
Mtσ^F	3.26	0.08	38.2		30
C47-AEDANS- Mtσ^F	2.99				
V19C/C47A-Mtσ^F	3.28	0.192	32.3		
V19C/C47A-AEDANS-Mtσ^F	2.65				
A6C/C47A-Mtσ^F	3.13	0.111	36	46	35
A6C/C47A-AEDANS-Mtσ^F	2.78				
L256C/C47A-Mtσ^F	2.79	0.04	43.2	57.5	33
L256C/C47A-AEDANS-Mtσ^F	2.67				

[a]The reported lifetime is the second-order average of a biexponential fit; $\tau_{av} = (\alpha_1\tau_1^2 + \alpha_2\tau_2^2)/(\alpha_1\tau_1 + \alpha_2\tau_2)$. [b]The distances were calculated using an R_0 of 25.4 Å. [c]Upper and lower limits of distances were calculated from steady-state anisotropy values by the method of Lakowicz (*17*).

As expected, the homology-modeled structure is highly helical and compact, reflecting the characteristics of the anti-sigma factor-bound Aaσ^{28} structure.

To compare the secondary structure of free Mtσ^F with that of the modeled structure, we have determined the far-UV circular dichroism spectra. Figure 6B shows the circular dichroism spectra of Mtσ^F. The helix content of the spectra can be estimated from the molar ellipticity value at 222 nm (*22*, *23*). The calculated helix content is ~25%. The helical content of the homology-modeled structure calculated by STRIDE is 66%, without the first 39 N-terminal residues. If one assumes that the first 39 residues are not helical, the predicted helix content will be 56%. This large deviation of measured helical content from the modeled value is indicative of significant disorder in the protein.

Intramolecular FRET in Free Mtσ^F. To have an understanding of how the free Mtσ^F structure differs from the modeled structure, we have attempted to compare several distances in the free Mtσ^F with that of the predicted homology-modeled structure. As the interpretation of distance estimates is dependent on whether the protein is a dimer or monomer in solution, we have undertaken a sedimentation equilibrium study. Figure 3B shows the ln C versus $r^2/2$ plot of the sedimentation equilibrium run. The calculated molecular mass from the slope is 31.6 kDa, characteristic of a monomer.

Interestingly, Mtσ^F has a single cysteine residue (C47) and a single tryptophan residue (W112), which is located in region 2.4. C47 was found to be reactive and can be labeled with fluorescence probes (data not shown). Fluorescence energy transfer between W112 (donor) and AEDANS-C47 (acceptor) was assessed in the time-resolved mode. The obtained distance (R) was approximately 37 Å (Table 1). This distance is considerably larger than the distance in the modeled structure (24 Å). However, uncertainties in κ^2 can be considerable, and a lower estimate of R (R_{min}) can be obtained from a Perrin plot and fluorescence anisotropy values of the donor and acceptor (*19*). The estimated R_{min} is approximately 30 Å, somewhat larger than the modeled distance. However, considering uncertainty in the modeled distance and flexibility of the probe linker, this value is not inconsistent with a compact structure.

Figure 7A shows emission spectra of wild-type Mtσ^F. The wild-type protein has emission maxima of around 341 nm, indicating that W112 is significantly shielded from solvent. This is consistent with a compact structure of the N-terminal half as in the homology-modeled structure. Figure 7B shows the acrylamide quenching of W112 in wild-type Mtσ^F. The Stern−Volmer

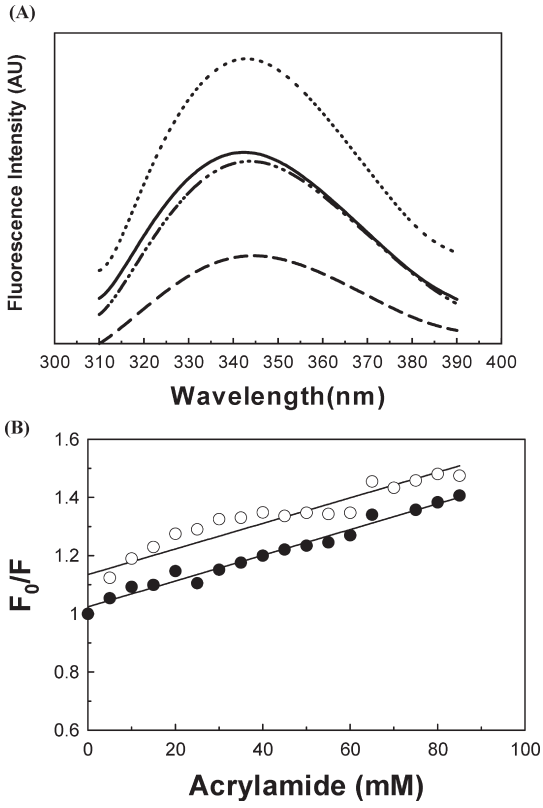

FIGURE 7: (A) Tryptophan emission scans of wild-type Mtσ^F and its mutants: (—) Mtσ^F, (---) V19C/C47A-Mtσ^F, (···) A6C/C47A-Mtσ^F, and (−·−) L256C/C47A-Mtσ^F. Protein concentrations were kept at 4.2, 3, 5, and 4 μM, respectively, for each in 0.05 M Tris-HCl buffer (pH 8.0) containing 0.2 M KCl and 20% glycerol. Excitation was set at 295 nm, and the scans are average of three scans. The excitation and emission band-passes were set at 5 nm. The scans were taken in a Photon Technology International spectrofluorometer. (B) Plot of F_0/F vs acrylamide concentration in 0.05 M potassium phosphate buffer (pH 8.0) containing 0.2 M KCl, 20% glycerol, 0.5 mM EDTA, and 1 mM β-mercaptoethanol. The protein concentrations were kept at 5 μM. The experiments were performed at 25 °C. The excitation wavelength was set at 295 nm, and the emission wavelengths were set at 341 and 343 nm for wild-type Mtσ^F (○) and L256C/C47A-Mtσ^F (●), respectively. The excitation and emission band-passes were set at 5 nm.

constant, K_{sv}, as determined from the slope is 4.4 M^{-1}. Because the lifetime of W112 is 3.27 ns (Table 1), the bimolecular quenching constant, k_q, is calculated to be 1.34×10^9 M^{-1} s^{-1}. This value is severalfold lower than the diffusion limit for free acrylamide and exposed tryptophan in proteins, indicating the shielded nature of W112. Thus, the region around W112 (region 2.4) appears to be compactly folded.

To visualize the spatial relationship of region 4.2 vis-à-vis region 2.4 of the protein, we have created a site-directed mutant, C47A/L256C. To create a unique probe attachment point, in all the mutant proteins in which a new cysteine residue is created, wild-type C47 is mutated to Ala. C47A/L256C-Mtσ^F was purified to homogeneity, and its emission spectrum was measured. The emission spectrum of C47A/L256C-Mtσ^F is very similar to that of wild-type Mtσ^F with emission maxima at 343 nm (Figure 7A). The Stern−Volmer plot is also very similar with a K_{sv} of 4.4 M^{-1} (Figure 7B). Given the similarity of the conformation around W112, one may assume that the conformation of the mutant protein is similar to that of the wild type. The distance between W112 and 256C was measured in time-resolved mode. The obtained distance was 43 Å. The lower limit of the

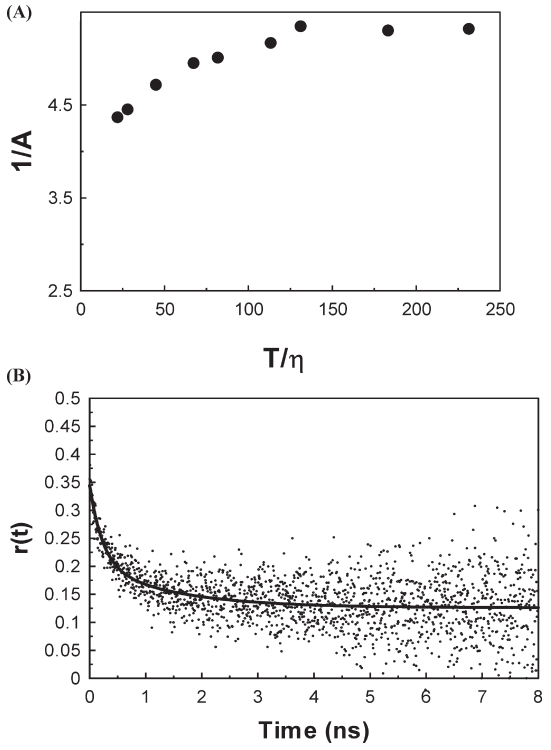

FIGURE 8: (A) Perrin plot of L256C/C47A-Mtσ^F. (B) Time-resolved anisotropy decay of L256C/C47A-Mtσ^F. The protein concentration for the Perrin plot was kept at 0.14 μM for each reading. The viscosity was varied isothermally by inclusion of glycerol in 0.05 M potassium phosphate buffer (pH 8.0). The temperature was 25 °C. For time-resolved anisotropy decay, the protein concentration was kept at 0.3 μM in 50 mM potassium phosphate buffer (pH 7.5) containing 300 mM KCl, 1 mM β-mercaptoethanol, and 20% glycerol.

distance is 0.73R, i.e., 33 Å. This is much longer than the modeled distance of 17 Å and probably beyond the range of deviations in the modeling and flexibility of the probe linker. This perhaps indicates the presence of a significant population of structures that are more open in nature in which the C-terminal part is farther from the N-terminal part. To determine if there is any internal motion around region 4.2, we have constructed the Perrin plot of L256C-labeled Mtσ^F. Figure 8A shows the Perrin plot of AEDANS-C47A/L256C-Mtσ^F. The plot appears to curve continuously. In the Perrin plot, if curvatures are seen, it is indicative of the presence of more than one rotational correlation time and, hence, internal mobility. The strong curvature seen here indicates very significant internal motion around region 4.2. This was verified by anisotropy decay measurements of Alexa 488-labeled L256C/C47A-Mtσ^F (Figure 8B). Anisotropy values that start around the theoretical maximum of 0.4 quickly decay to around 0.12 within 8 ns. The decay can be fitted to two correlation times of 0.23 and 1.43 ns, indicating rapid internal motion. A longer correlation time may be present, but a higher signal-to-noise ratio is necessary at longer times to resolve that. However, large depolarization in the early time window (almost 70%) is a definitive indication of significant internal motions. Given that the actual distance of L256 is at least double that of the modeled distance and the L256-containing segment has considerable internal motion, it is likely that the C-terminal part of Mtσ^F is flexible and does not always form a compact structure. Thus, a picture of free Mtσ^F emerges in which a large part of the N-terminal part is folded and compact, whereas the C-terminal half may be somewhat disordered.

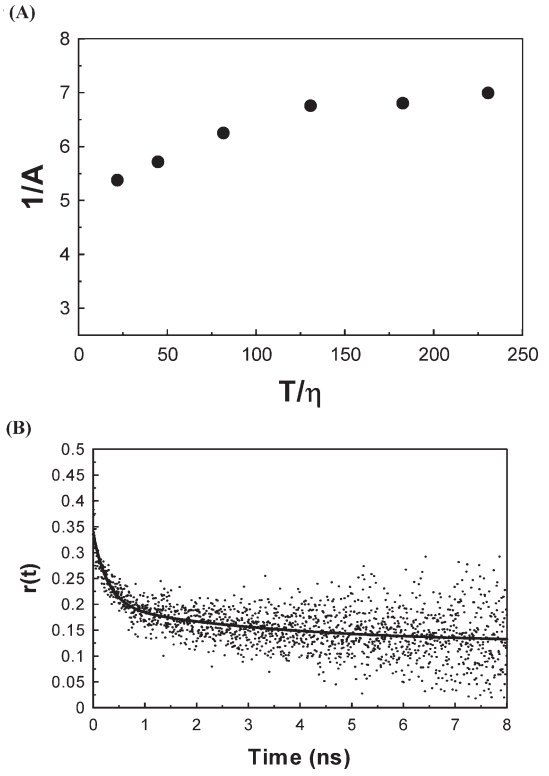

FIGURE 9: (A) Perrin plot of A6C/C47A-Mtσ^F. (B) Time-resolved anisotropy decay of A6C/C47A-Mtσ^F. Details are given in the legend of Figure 8 and Experimental Procedures.

Nature of Region 1.2 of Mtσ^F. The role of region 1 of sigma factors, including those of region 1.1 in the σ^{70} family, is not totally clear. Some sigma factors lack a recognizable region 1.1 altogether. Even when region 1 is very short in some sigma factors, they seem to play important role in the transcription process (*26*). Overall, it appears that region 1 may play an important role in all sigma factors, although the roles may be somewhat different. We, thus, explored the dynamics and position of region 1 of Mtσ^F using fluorescence spectroscopy. We have created two site-directed mutants, C47A/V19C-Mtσ^F and C47A/A6C-Mtσ^F, putting reactive single cysteines in region 1. The mutant proteins were labeled with IAEDANS, and fluorescence resonance energy transfer from W112 was measured in time-resolved mode. Table 1 lists the energy transfer efficiencies and the corresponding distances. The distances of both the N-terminal residues are between 30 and 45 Å (counting the estimated uncertainties) from W112. Although neither residue is visible in the homology-modeled structure, the N-terminal residue in the modeled structure, R40, is ~40 Å from W112. If region 1.2 is free to move, the distance between residues 112 and 6 would be considerably longer. This suggests that region 1 may fold over and interact with the main folded part of the protein containing region 2.4. This is consistent with conclusions derived by Muir and co-workers (*4*). We have also constructed a Perrin plot for AEDANS-C47A/A6C-Mtσ^F labeled at C6 (Figure 9A). The plot here is also somewhat curved and thus indicative of significant internal motion. This was also verified by anisotropy decay experiments (Figure 9B). The decay here can be fitted to correlation times of 0.29 and 3.52 ns. It thus may be concluded that the first 40 residues of Mtσ^F (region 1) may have very significant mobility but at the same time interact with the main folded part of the protein.

DISCUSSION

The picture that emerges from the study of Ecσ^{32} is that the protein is largely well ordered and compact in solution. In this conformation, region 4.2 comes near the folded N-terminal region containing region 2.4. Darst and co-workers have compared the structure of free and anti-sigma factor-bound Aaσ^{28} in solution using strategically placed cysteine residues and comparing the disulfide formation in the presence and absence of the anti-sigma factor (*5*). Their data can be interpreted like those of Ecσ^{32}; free Aaσ^{28} must have a crystal-like compact conformation, at least to a large extent. However, in Ecσ^{32}, a previous H−D exchange study clearly demonstrated that the amide protons in the C-terminal half have little protection from solvent exchange (*6*). Clearly, there must be states in equilibrium with the compact folded form, from which rapid hydrogen exchange can occur. This degree of flexibility is consistent with variations in anisotropy seen at different positions of the protein. This flexibility may be local in nature (i.e., intradomain) or could be a conformational equilibrium between a compact and a globally open form (i.e., interdomain). Although the data presented here cannot distinguish between the two alternatives, we prefer the latter alternative because of the lack of protection of amide protons in many regions of the protein as well as decreased anisotropy in more than one region. Thus, a more realistic picture may be proposed in which a compact Aaσ^{28}-like form (the predominant conformation) is in equilibrium with a more open exposed and/or disordered conformation. However, this putative interdomain motion can be in the presence of local intradomain motion as well. In a recent article, a detailed H−D exchange experiment in the presence and absence of DnaK led to the hypothesis that Ecσ^{32} may be in an equilibrium of two conformations (*27*).

In the other homologous sigma factor, Mtσ^{F}, spectroscopic data suggest the presence of a folded N-terminal domain around region 2.4 as well. Like Ecσ^{32}, Mtσ^{F} also appears to possess significant mobility in region 1.2 and region 4.2 but appears to be even less compact. What is the relationship between the overall structure and significant internal mobility? The estimate obtained from FRET experiments for the distance between an N-terminal residue in region 2.4 and a C-terminal residue in region 4.2 in Mtσ^{F} shows significant deviations from distances in the modeled structure having a compact conformation. At the same time, the distance is also not compatible with a fully disordered structure. The circular dichroism spectrum is also consistent with significant disorder. This implies the presence of significant population of structures that are more open than the compact homology-modeled structure. Thus, a more realistic picture is that an open partially disordered form is in equilibrium with a more compact folded form like the homology-modeled structure, with the latter being the predominant population.

For Aaσ^{28}, no data on flexibility are available. However, the rate of disulfide formation is not incompatible with the presence of a minor population of a more open structure. Experimental data reported for all three sigma factors can be reconciled with a model in which a compact Aaσ^{28} crystal structure-like form is in equilibrium with one or more open forms in which the C-terminal half is not packed against the folded N-terminal domain. The position of the equilibrium and the degree of disorder in the C-terminal half may vary somewhat in the case of each sigma factor, although it appears that the compact form is the predominant conformation. Interestingly, region 1 appears to have

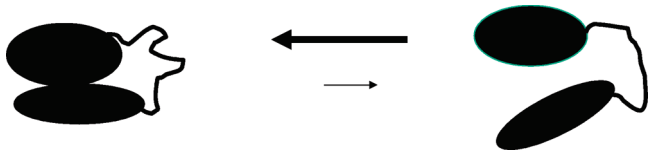

FIGURE 10: Cartoon figure depicting the proposed equilibrium of two conformations of the sigma factors.

significant freedom in Ecσ^{32} and possibly more freedom in Mtσ^{F}. It is tempting to speculate that the disorder in the C-terminal half is correlated with flexibility region 1. Thus, interaction of region 1 may promote a compact conformation in which regions 2.4 and 4.2 are in a conformation not ready for promoter binding. Elimination of this N-terminal region enhances the flexibility of the sigma factor and the population of the open form and hence promotes moderate recognition of the promoters seen in some experiments (*1*). This model is depicted in cartoon form in Figure 10.

Why then do all the studied sigma factors have considerable flexibility? One possibility may be that the inherent flexibility may help in the conformational switch needed to bind to the core enzyme. The flexibility may reduce the energetic cost of the conformational change before binding to the core enzyme. If some of this inherent flexibility of region 4.2 is preserved in the holoenzyme, it may also help this region to adapt to different promoter geometry and contact the regulatory proteins bound to different regulatory binding sites. In addition, the sigma factors interact with many other proteins such as anti-sigma factors and chaperones as part of complex regulatory pathways. Such flexibility may be essential to participation in such complex regulatory cycles. In a series of recent articles, it was pointed out that alternative sigma factors have a more extended region of promoter recognition (−10, extended −10 and −35), possibly to create a more stringent recognition system (*28*−*30*). This extended initial contact may require significant remodeling of the sigma factor structure where flexibility may be crucial.

ACKNOWLEDGMENT

We acknowledge Prof. Kankan Bhattacharyya and the picosecond national time-resolved facility of the Indian Association for the Cultivation of Science in Kolkata, India, for the anisotropy decay measurements. We also acknowledge Dr. Samir Pal for helping us with the anisotropy decay measurements.

SUPPORTING INFORMATION AVAILABLE

Sulfhydryl reactivity profile (Figure 1). This material is available free of charge via the Internet at http://pubs.acs.org.

REFERENCES

1. Dombroski, A. J., Walter, W. A., and Gross, C. A. (1993) Amino-terminal amino acids modulate sigma-factor DNA-binding activity. *Genes Dev. 7*, 2446–2455.
2. Dombroski, A. J., Walter, W. A., Record, M. T., Jr., Siegele, D. A., and Gross, C. A. (1992) Polypeptides containing highly conserved regions of transcription initiation factor sigma 70 exhibit specificity of binding to promoter DNA. *Cell 70*, 501–512.
3. Camarero, J., Shekhtman, A., Campbell, E., Chlenov, M., Gruber, T., Bryant, D., Darst, S., Cowburn, D., and Muir, T. (2002) Autoregulation of a bacterial factor explored by using segmental isotopic labeling and NMR. *Proc. Natl. Acad. Sci. U.S.A. 99*, 8536–8541.
4. Schwartz, E., Shekhtman, A., Dutta, K., Pratt, M., Cowburn, D., Darst, S., and Muir, T. (2008) A full-length group 1 bacterial sigma factor adopts a compact structure incompatible with DNA binding. *Chem. Biol. 15*, 1091–1103.

5. Sorenson, M., and Darst, S. (2006) Disulfide cross-linking indicates that FlgM-bound and free 28 adopt similar conformations. *Proc. Natl. Acad. Sci. U.S.A. 103*, 16722–16727.
6. Rist, W., Jørgensen, T., Roepstorff, P., Bukau, B., and Mayer, M. (2003) Mapping temperature-induced conformational changes in the *Escherichia coli* heat shock transcription factor 32 by amide hydrogen exchange. *J. Biol. Chem. 278*, 51415–51421.
7. Liu, J., Perumal, N., Oldfield, C., Su, E., Uversky, V., and Dunker, A. (2006) Intrinsic Disorder in Transcription Factors. *Biochemistry 45*, 6873–6888.
8. Ho, S., Hunt, H., Horton, R., Pullen, J., and Pease, L. (1989) Site-directed mutagenesis by overlap extension using the polymerase chain reaction. *Gene 77*, 51–59.
9. Tate, W., Poole, E., Dalphin, M., Major, L., Crawford, D., and Mannering, S. (1996) The translational stop signal: Codon with a context, or extended factor recognition element? *Biochimie 78*, 945–952.
10. Joo, D. M., Ng, N., and Calendar, R. (1997) A sigma32 mutant with a single amino acid change in the highly conserved region 2.2 exhibits reduced core RNA polymerase affinity. *Proc. Natl. Acad. Sci. U.S.A. 94*, 4907–4912.
11. Haugland, R. (1992) Handbook of Fluorescent probes and Research Chemicals, Molecular Probes, Eugene, OR.
12. Weast, R. (1977) CRC Handbook of Chemistry and Physics, 57th ed., CRC Press, Boca Raton, FL.
13. Bhattacharya, A., Bhattacharyya, B., and Roy, S. (1996) Fluorescence energy transfer measurement of distances between ligand binding sites of tubulin and its implication for protein-protein interaction. *Protein Sci. 5*, 2029–2036.
14. Sorenson, M., Ray, S., and Darst, S. (2004) Crystal Structure of the Flagellar σ/Anti-σ Complex σ28/FlgM Reveals an Intact σ Factor in an Inactive Conformation. *Mol. Cell 14*, 127–138.
15. Paget, M., and Helmann, J. (2003) The sigma70 family of sigma factors. *Genome Biol. 4*, 2003–2004.
16. Lonetto, M., Gribskov, M., and Gross, C. A. (1992) The sigma 70 family: Sequence conservation and evolutionary relationships. *J. Bacteriol. 174*, 3843–3849.
17. Chattopadhyay, R., and Roy, S. (2002) DnaK-sigma 32 interaction is temperature-dependent. Implication for the mechanism of heat shock response. *J. Biol. Chem. 277*, 33641–33647.
18. Kuznedelov, K., Minakhin, L., Niedziela-Majka, A., Dove, S., Rogulja, D., Nickels, B., Hochschild, A., Heyduk, T., and Severinov, K. (2002) A role for interaction of the RNA polymerase flap domain with the sigma subunit in promoter recognition. *Science 295*, 855–857.
19. Lakowicz, J. R. (1999) Principles of fluorescence spectroscopy, 2nd ed., Kluwer Academic/Plenum Publishers, New York.
20. Vassylyev, D., Sekine, S., Laptenko, O., Lee, J., Vassylyeva, M., Borukhov, S., and Yokoyama, S. (2002) Crystal structure of a bacterial RNA polymerase holoenzyme at 2.6 Å resolution. *Nature 417*, 712–719.
21. Heinig, M., and Frishman, D. (2004) STRIDE: A web server for secondary structure assignment from known atomic coordinates of proteins. *Nucleic Acids Res. 32*, W500–W502.
22. Sparks, D., Lund-Katz, S., and Phillips, M. (1992) The charge and structural stability of apolipoprotein AI in discoidal and spherical recombinant high density lipoprotein particles. *J. Biol. Chem. 267*, 25839–25847.
23. Morrow, J., Segall, M., Lund-Katz, S., Phillips, M., Knapp, M., Rupp, B., and Weisgraber, K. (2000) Differences in Stability among the Human Apolipoprotein E Isoforms Determined by the Amino-Terminal Domain. *Biochemistry 39*, 11657–11666.
24. Yguerabide, J. (1972) Nanosecond fluorescence spectroscopy of macromolecules. *Methods Enzymol. 26*, 498–578.
25. Banik, U., Mandal, N. C., Bhattacharyya, B., and Roy, S. (1993) A fluorescence anisotropy study of tetramer-dimer equilibrium of lambda repressor and its implication for function. *J. Biol. Chem. 268*, 3938–3943.
26. Cantor, C., and Schimmel, P. (1980) Biophysical chemistry: Part II: Techniques for the study of biological structure and function, W. H. Freeman & Co., New York.
27. Rodriguez, F., Ars ne-Ploetze, F., Rist, W., Rüdiger, S., Schneider-Mergener, J., Mayer, M., and Bukau, B. (2008) Molecular Basis for Regulation of the Heat Shock Transcription Factor σ32 by the DnaK and DnaJ Chaperones. *Mol. Cell 32*, 347–358.
28. Koo, B., Rhodius, V., Campbell, E., and Gross, C. (2009) Dissection of recognition determinants of *Escherichia coli* σ32 suggests a composite-10 region with an 'extended-10' motif and a core-10 element. *Mol. Microbiol. 72*, 815–829.
29. Koo, B., Rhodius, V., Campbell, E., and Gross, C. (2009) Mutational analysis of *Escherichia coli* 28 and its target promoters reveals recognition of a composite-10 region, comprised of an 'extended-10' motif and a core-10 element. *Mol. Microbiol. 72*, 830–843.
30. Feklistov, A., and Darst, S. (2009) Promoter recognition by bacterial alternative factors: The price of high selectivity? *Genes Dev. 23*, 2371–2375.